JOURNAL OF CATALYSIS 12, 172–182 (1968)

Chemisorption Rates by Chromatography

GÜNTER PADBERG AND J. M. SMITH

From the University of California, Davis, California 95616

Received June 10, 1968; revised August 14, 1968

Using chromatography, rates of chemisorption of hydrogen on a nickel catalyst were measured at 1 atm pressure and 243–297°K. The method depends upon analyzing the response to a pulse of deuterium added to a stream of hydrogen flowing through the catalyst bed. The bed has previously been exposed to hydrogen so that all adsorbable surface has been occupied. Thus the measurements were made at constant surface coverage. At these equilibrium conditions the rates of adsorption and desorption are identical.

The observed activation energy was 13.8 kcal/mole. This is about the same as the isosteric heat of adsorption given in the literature. Also it was shown that the observed activation energy should be nearly equivalent to that for desorption. Hence the adsorption process appears to be essentially nonactivated.

Based upon recent theory, a method has been developed [Schneider and Smith (*1*), (*2*)] for establishing rate and equilibrium parameters from chromatographic curves. The method can be used to evaluate adsorption equilibrium constants, axial diffusivities, intraparticle diffusitives, and adsorption rate constants. These authors illustrated the method by studies of the physical adsorption of hydrocarbons. For these systems the rate of the overall process was controlled by intraparticle diffusion.

It would be valuable to be able to use the technique for studying rates of chemisorption. However, the crucial point in the method is that all processes involved must be describable by linear equations. For chemisorption this requirement will probably never be fulfilled: at higher surface coverage adsorption isotherms are nonlinear, and at very low surface coverage surface heterogeneity will cause deviations from linearity. This latter phenomenon leads to "tailing" of peaks in adsorption chromatography.

However, there is a method to overcome these difficulties—application of an isotopic tracer. By this procedure the adsorption rate can be measured at equilibrium conditions (constant surface coverage). In this work the chemisorption of hydrogen on a porous nickel-kieselguhr catalyst was studied. The chromatographic column contained the catalyst, hydrogen was used as carrier gas, and pulses of deuterium were introduced as a tracer. From chromatographic measurements in the same system Ozaki and co-workers (*3*, *4*) found that hydrogen chemisorption on nickel is largely reversible, and they determined the amount of such adsorption. From their work it was concluded that rates of chemisorption in this system could be measured by chromatography.

NOTATIONS

C	Concentration of the tracer in the interparticle space (mole/cm³)
C_i	Concentration of the tracer in the catalyst pores (mole/g)
C_g	Total concentration in the gas phase (moles/cm³ or molecules/cm³)
D_{AB}	Binary molecular diffusivity (cm²/sec)
D_c	Effective intraparticle diffusivity (cm²/sec)
D_K	Knudsen diffusivity (cm²/sec)
E_a, E_d	Activation energies of adsorption and desorption (cal/mole)
E_A	Effective axial diffusivity (cm²/sec)
$f^\ddagger$	Partition function for activated

	surface complex (without the critical vibration)
f_{s2}, f_{a2}	Partition functions for dual bare and dual covered surface sites
F_g	Partition function for the gas per cm^3 (cm^{-3})
h	Planck's constant [erg(sec)]
k	Boltzmann's constant (erg/°K)
k_a	Adsorption rate constant (cm^3/g sec)
K_a	Adsorption equilibrium constant (cm^3/g)
k_f	Mass-transfer coefficient (cm/sec)
M	Molecular weight (g/mole)
m_n	Defined by Eq. (13)
n_a	Amount of tracer adsorbed (mole/g)
n_s	Number of nickel surface sites per cm^2 (cm^{-2})
q	Heat of adsorption (cal/mole)
q_{ext}	Tortuosity factor of packed bed
r	Distance from center of spherical particle (cm)
R	Radius of spherical catalyst particle (cm)
r_a, r_d	Rates of adsorption and desorption (molecules/cm^2 sec)
$\bar{r}_i, \bar{r}_a$	Average radii of micropores and macropores in the catalyst (cm)
R_g	Gas constant
t	time (sec)
t_0	Injection time of tracer pulse (sec)
T	Temperature (°K)
v	Linear gas velocity in the interparticle space (cm/sec)
z	Length coordinate in the catalyst bed, from inlet (cm)
α	Void fraction of the catalyst bed
β	Porosity of catalyst particle
β_a, β_i	Porosities of catalyst particle due to macropores and micropores
δ_0, δ_1	Defined by Eqs. (17) and (18)
φ_a, φ_d	Probabilities of two adjacent surface sites being bare or covered by adsorbed atoms (at a fixed surface coverage)
μ'_n, μ_n	nth absolute and central moment of the chromatographic curve [Eqs. (12) and (14)]
ρ_p	Apparent density of catalyst particle (g/cm^3)
θ	Surface coverage

The Tracer Method

It is well known that hydrogen atoms are the adsorbed species on nickel surfaces. In an isothermal hydrogen stream the nickel particles in the column will reach a steady state of surface saturation. Now assume a deuterium pulse is introduced. If the hydrogen on the surface and in the gas are in dynamic equilibrium, deuterium also has a chance to be chemisorbed. This causes the deuterium pulse to be retained in the column, and the retention time is a measure of the equilibrium distribution between the gas phase and the nickel surface. Since chemisorption in this system is dissociative, the adsorption–desorption process will tend to establish equilibrium in the exchange reaction $H_2 + D_2 = 2HD$ in the gas phase.

If the isotope effect on the rates is negligible, the rate of adsorption of deuterium is equal to the total rate of adsorption multiplied by the mole fraction of deuterium in the gas. Similarly, the rate of desorption of deuterium is proportional to the mole fraction of deuterium atoms on the surface, relative to the total of hydrogen plus deuterium atoms adsorbed. Since the pressure is constant, and the overall hydrogen plus deuterium system remains in equilibrium at all times, the total rates are constant. At constant surface coverage we can, therefore, use a linear equation for the net rate of adsorption of the tracer:

$$dn_a/dt = r_a - r_d = k_a C - (k_a/K_a) n_a \quad (1)$$

where

$$K_a = k_a/k_d = (n_a/C)_{equil}\ cm^3/g \quad (2)$$

and n_a is the concentration of the adsorbed deuterium, mole/gram of catalyst.

In order to be independent of whether the deuterium in the gas phase is present as D_2 or HD, the deuterium concentration is defined by

$$C = \tfrac{1}{2} C_{HD} + C_{D_2}\ mole/cm^3 \quad (3)$$

Note that the linear equations (1) and (2) are only valid for the tracer component and at a constant concentration of "total hydrogen." Thus Eq. (2) is applied to but one point of the (nonlinear) adsorption

isotherm corresponding to the particular total concentration used. Thus, K_a is not independent of concentration but simply the ratio given by Eq. (2) at a point in the nonlinear section of the isotherm. Similarly Eq. (1) corresponds to only one value for the rates at that concentration. Since the overall system remains always in equilibrium, the total rate of adsorption equals the total rate of desorption. To gain more information on the nonlinear "total hydrogen" system one would have to carry out experiments at different pressures.

The underlying assumption of a negligible isotope effect is, in the case of hydrogen isotopes, only an approximation (*5*, *6*), but experiments described later show that the linearity conclusions are still rather well satisfied.

Method of Analysis

Since a complete description of the method is available (*1*) only a brief summary is given here.

At constant pressure conservation equations for one tracer component in a continuous flow of the carrier gas, through a column filled with spherical adsorbent particles, are as follows:

(1) the mass balance in the interparticle space

$$\frac{E_A}{\chi}\frac{\partial^2 C}{\partial z^2} - v\frac{\partial C}{\partial z} - \frac{\partial C}{\partial t} - \frac{3D_c}{R}\frac{1-\alpha}{\alpha}\left(\frac{\partial C_i}{\partial r}\right)_{r=R} = 0 \quad (4)$$

(2) the mass balance in the spherical porous particle

$$\frac{D_c}{\beta}\left(\frac{\partial^2 C_i}{\partial r^2} + \frac{2}{r}\frac{\partial C_i}{\partial r}\right) - \frac{\partial C_i}{\partial t} - \frac{\rho_p}{\beta}\frac{\partial n_a}{\partial t} = 0 \quad (5)$$

(3) the rate of adsorption and desorption, given by Eq. (1)

(4) the external diffusion boundary condition

$$D_c\left(\frac{\partial C_i}{\partial r}\right)_{r=R} = k_f(C - C_i) \quad (6)$$

(5) the internal diffusion boundary condition

$$\partial C_i/\partial r = 0 \quad \text{at } r = 0 \quad \text{for } t \geq 0 \quad (7)$$

(6) the initial conditions

$$C = 0 \quad \text{at } z > 0 \quad \text{for } t = 0 \quad (8)$$

$$C_i = 0 \quad \text{at } r \geq 0 \quad \text{for } t = 0 \quad (9)$$

(7) the function $C(0,t)$, giving the pulse input of the tracer

$$C = C_0 \quad \text{at } z = 0 \quad \text{for } 0 \leq t \leq t_0 \quad (10)$$

$$C = 0 \quad \text{at } z = 0 \quad \text{for } t > t_0 \quad (11)$$

Kubin (*7*, *8*) solved this system of equations and arrived at useful expressions for the statistical moments of the chromatographic curves. The nth absolute moment of the function $C(z,t)$ is defined

$$\mu'_n = m_n/m_0 \quad (12)$$

where

$$m_n = \int_0^\infty t^n C(z,t)\, dt \qquad (n = 0,1,2 \ldots) \quad (13)$$

The nth central moment is defined as

$$\mu_n = \frac{1}{m_0}\int_0^\infty (t - \mu'_1)^n C(z,t)\, dt \qquad (n = 2,3 \ldots) \quad (14)$$

The equations given by Kubin for the first moment and the second central moment are

$$\mu'_1 = \left(\frac{z}{v}\right)(1 + \delta_0) + \frac{t_0}{2} \quad (15)$$

$$\mu^2 = \left(\frac{2z}{v}\right)\left[\delta_1 + \left(\frac{E_A}{\alpha}\right)(1 + \delta_0)^2\left(\frac{1}{v^2}\right)\right] + \frac{t_0^2}{12} \quad (16)$$

where

$$\delta_0 = \left[\frac{(1-\alpha)\beta}{\alpha}\right]\left[1 + \left(\frac{\rho_p}{\beta}\right)K_a\right] \quad (17)$$

$$\delta_1 = \frac{1-\alpha}{\alpha}\beta\left[\frac{\rho_p}{\beta}\frac{K_a^2}{k_a} + \frac{R^2\beta}{15}\left(1 + \frac{\rho_p}{\beta}K_a\right)^2\left(\frac{1}{D_c} + \frac{5}{k_f R}\right)\right] \quad (18)$$

The rate and equilibrium constants, E_A, D_c, k_a, and K_A can be evaluated from Eqs. (15)–(18), if the first and second moments are measured experimentally as

a function of carrier gas velocity and particle size.

Since the physical properties of the bed are known, the first moments give immediately the adsorption equilibrium constant K_a [Eqs. (15) and (17)]. For experiments at low Reynolds' numbers the axial diffusivity E_A and the mass-transfer coefficient k_f are independent of gas velocity. Then plots of $(\mu_2 - t_0^2/12)/(2z/v)$ versus $1/v^2$ will yield straight lines. From the slopes of these lines and the known K_a, E_A can be calculated. The intercepts in these plots, δ_1, give the combined contributions to the second moment due to (1) the finite rates of adsorption and desorption; (2) the diffusion within the porous pellets; (3) the diffusion to the outer surface of the pellet.

In the low-velocity region the expression $k_f R$ can be replaced by the bulk diffusivity D_{AB} (*1*). If the intercepts δ_1 are evaluated for different particle radii R, a graph of $\delta_1/[(1-\alpha)\beta/\alpha]$ versus R^2 should give a straight line. From the intercept (at $R^2 = 0$), which is a measure of the adsorption resistance, k_a can be calculated. The slope reflects the resistance due to internal and external diffusion so that D_e can be determined. In evaluating D_e the external mass-transfer resistance is taken into account, but this resistance is very small at chromatographic conditions.

The moments of the experimental chromatographic curves reported later were evaluated from Eqs. (13) and (14) using Simpson's rule and machine computation

Experimental

With hydrogen as carrier gas and deuterium as sample gas, chromatographic curves were measured at atmospheric pressure for three particle sizes (R = 0.114, 0.229, and 0.324 mm) at temperatures of 24°, 0°, −7.5°, and −15°C, and, for the smallest particle size, also at −22.5° and −30°C. A number of experiments with different carrier gas velocities was made for each temperature and particle size. The linear gas velocities in the interparticle space ranged from 5 to 20 cm/sec.

Some measurements were carried out using hydrogen as carrier gas and helium as nonadsorbable sample gas. This was done to obtain first and second moments for an inert gas and to determine the dead volume between sampling device and detector.

Apparatus. The apparatus was essentially a conventional gas chromatograph. The gas flows were regulated and kept constant by means of needle valves and differential pressure controllers. The sampling device (Aerograph 7-Port Gas Sample Valve) permitted injection of square-wave samples of different volumes; unless otherwise mentioned the sample volume was 0.5 cm³. Analysis of the gas mixture leaving the column was made with a thermal conductivity detector. The gas lines connecting the column to the sample valve and the detector consisted of 20 cm long, 1/16 inch stainless steel tubing (ID 1 mm). Without disconnecting the column from the H_2 stream, it could be placed in either a furnace for high-temperature treatment of the catalyst, or in the constant (low) temperature bath for the chromatographic runs. This temperature control within the latter was within ± 0.3°C. Gas flows were measured with a soap-bubble flow meter.

Gases. The hydrogen (prepurified) had a purity of better than 99.95%; traces of oxygen were removed by passing the stream through a bed of an oxidation catalyst (Engelhard DEOXO-purifier) and then through a drying column. The deuterium was technical grade with a stated D_2 content of 98%. The helium had a stated purity of 99.99%.

Catalyst and columns. The nickel catalyst was G-49B, nickel on kieselguhr from the Girdler Company. As sold it contained 47.9% nickel with 56.2% of the nickel in reduced form. The catalyst tablets were crushed and the resulting particles size-graded with standard sieves. The sieves were chosen so that the particle diameters in each fraction varied less than ±10% from the average value.

Before use the catalyst was reduced for 14 hr in the chromatographic column in a H_2 stream at 350°C. After reduction a small hydrogen stream was always flowing through the column to prevent contamination of the highly active and pyrophoric

TABLE 1
PROPERTIES OF THE CATALYST

Nickel content in reduced catalyst	50 wt %
Apparent particle density	ρ_p = 1.73 g/cm³
Total particle porpsity	β = 0.58
Surface area (BET)	S_t = 205 m²/g*
Porosity due to pores of radii 15–150 Å	β_i = 0.38*
Average pore radius of micropores	$\bar{r}_i$ = 25 Å*
Porosity due to pores of radii 150–10,000 Å	β_a = 0.20*
Average pore radius of macropores	$\bar{r}_a$ = 870 Å*
Nickel surface area per gram of catalyst	S_{Ni} = 42.3 m²/g
Average nickel crystal diameter, $\bar{d} = 6V_{Ni}/S_{Ni}$	$\bar{d}$ = 80 Å

particles. Table 1 gives the most important physical data for the catalyst.

Values marked with an asterisk were determined with the catalyst dried in a He stream at 220°C, but not completely reduced. These properties are not expected to be very sensitive to the final reduction. The total surface area was calculated by the BET method from the nitrogen adsorption isotherm. The pore-size distribution for radii of 150 Å and less was calculated from the desorption branch of the isotherm in the capillary condensation region (*9*). The nitrogen adsorption measurements were. made at liquid nitrogen temperature using the flow method (Perkin-Elmer Sorptometer). The pore-size distribution for radii greater than 150 Å was determined from data of mercury penetration vs. pressure, obtained in an Aminco porosimeter. The distribution for this catalyst shows two maxima, which probably originate from preparing the catalyst tablets by compressing small particles. The average pore radii for micorpores and macropores ($\bar{r}_i$,$\bar{r}_a$) in Table 1 were calculated by integration of the distributions of pore radii over the pore volume.

To estimate the *nickel* surface area of the catalyst the H_2 adsorption isotherm was measured in a conventional vacuum apparatus. A catalyst sample was reduced *in situ* in flowing H_2 at 350°C for 14 hr, and then evacuated at 350°C for 5 hr (with a mercury diffusion pump) before measuring the isotherm at 25°C. The amount adsorbed increased from 4.88×10^{-4} mole/g at 100 torr to 5.24×10^{-4} mole/g at 450 torr. If the last value is assumed to correspond to complete surface coverage, and 6.7 Å² is used for the area of a nickel surface atom (*10*), the nickel area is 42.3 m²/g of catalyst. From this area and the volume of nickel per gram of catalyst, V_{Ni}, the average size (80 Å) of the nickel crystals is obtained.

The properties of the columns are given in Table 2. They were made by packing

TABLE 2
BED CHARACTERISTICS

Column	Mass of catalyst (g)	Bed void fraction, α	Particle radius (mm)
I	7.40	0.370	0.114
II	7.12	0.393	0.229
III	7.22	0.387	0.324

1/4 inch copper tubing (ID, 4.81 mm). The packed bed length was 37.4 cm for all runs.

RESULTS AND DISCUSSION

Linearity of the System

Figure 1 illustrates the type of chromatographic peaks obtained, with H_2 as carrier and D_2 as sample gas, for three different temperatures. These curves were measured

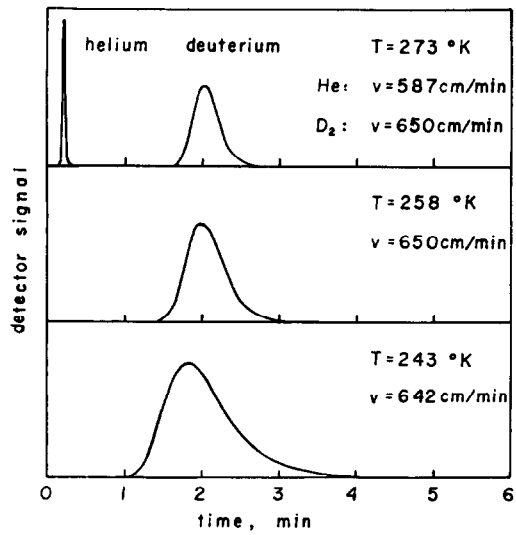

FIG. 1. Typical chromatographs (Column I).

with Column I (see Table 2) and are for about the same carrier gas velocity. For $T = 273°K$ a helium peak is also shown, demonstrating the behavior of a nonadsorbing sample. Figure 1 shows that the position of the deuterium peaks is only slightly affected by a variation of temperature from 273° to 243°K, whereas the width and the shape of the curves are considerably changed. Since the temperature dependency of transport processes is too small to produce such an effect, it was anticipated that the finite rate of chemisorption was responsible. However, it is critical to verify that this broadening and tailing could not result from a nonlinear equilibrium relation. So experiments were run with different samples sizes, all other conditions kept constant. Table 3 gives the resulting

TABLE 3
EFFECT OF PULSE VOLUME ON MOMENTS

Experimental conditions	Sample volume (cm³)	First moment (min)	Second, central moment (min²)
a	0.33	2.762	6.10×10^{-2}
a	0.50	2.756	6.18×10^{-2}
a	1.30	2.727	6.31×10^{-2}
a	2.36	2.705	6.26×10^{-2}
b	0.33	2.925	0.126
b	0.50	2.909	0.127
b	1.30	2.886	0.130
b	2.36	2.863	0.126

[a] Column I, $v = 495$ cm/min, $T = 273°K$.
[b] Column I, $v = 468$ cm/min, $T = 258°K$.

first absolute and second central moments, as a function of sample volume, for two temperatures. The first moments decrease slightly (by about 3%), and the second central moments scatter within ±2% of an average value, as the sample volume increases from 0.33 to 2.36 cm³. Thus the position and the shape of the chromatographic curve remains essentially the same when the concentration of the peak varies over a sevenfold range. This is evidence that the linear rate and equilibrium equations expected for the tracer component are fulfilled, within the accuracy of the experimental technique.

Adsorption Equilibrium Results

Combining Eqs. (15) and (17) gives

$$\mu'_1 = \frac{z}{v}\left(1 + \frac{1-\alpha}{\alpha}\beta\right) + \frac{z}{v}\left(\frac{1-\alpha}{\alpha}\beta\right)\frac{\rho_p}{\beta}K_a + \frac{t_0}{2} \quad (15a)$$

The first expression on the right side is the first moment of an inert gas μ'_1 (inert). With $\Delta\mu'_1 = \mu'_1 - \mu'_1$ (inert) a plot of $(\Delta\mu'_1 - t_0/2)/[(1-\alpha)\beta/\alpha]$ versus z/v will yield a straight line with a slope equal to $(\rho_p/\beta)K_a$. This expression for μ'_1 (inert) accounts only for the gas space in the catalyst bed. Since there is a certain additional dead volume between the catalyst bed and both the sample valve and the detector, the total dead volume was determined from the first moments of helium peaks. Thus μ'_1 (inert) was calculated for each run as μ'_1 (inert) = $V_{dead}/\dot{V}$, where $\dot{V}$ is the volumetric flow rate.

Figure 2 gives an example of first-moment plots at 24°C. The points for the different particle sizes should fall on one line. This was true for the two bigger particle sizes, whereas the slope for the smallest particle

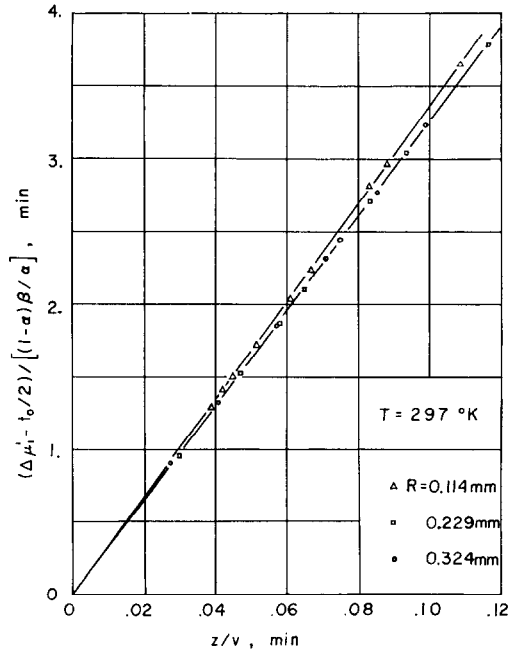

FIG. 2. First moment at 297°K.

TABLE 4
ADSORPTION EQUILIBRIUM CONSTANTS

Temp. (°K)	297	273	265.5	258	250.5	243
K_a(cm³/g)	11.1	10.9	10.9	10.9	10.8	10.9
$10^4 n_a$(mole/g)	4.55	4.86	5.00	5.15	5.25	5.46

was about 3% steeper at all temperatures. This small deviation in adsorption capacity is probably due to a slightly different catalyst pretreatment. An average value of K_a for all three particle sizes was used. Table 4 shows the results. As noted earlier, these K_a values are not true adsorption equilibrium constants in that they do not apply to the linear portion of the isotherm. In the last row $n_a = K_a\ C_{total}$ is given, where C_{total} is the gas concentration at atmospheric pressure and column temperature. In the absence of an isotope effect, this would be equal to the amount of hydrogen reversibly adsorbed at atmospheric pressure. It is seen that this value decreases slightly with increasing temperature, and so does the surface coverage of the nickel. Due to the nature of the method, these figures can only include that hydrogen on the surface which is readily exchangeable. It is interesting to compare these results with the hydrogen uptake of the catalyst after evacuation at 350°C (see catalyst properties). At 1 atm and 25°C the hydrogen adsorption isotherm gives an extrapolated value of 5.5×10^{-4} vs. 4.55×10^{-4} mole/g from Table 4. Thus about 80% of the hydrogen atoms, which can be removed by pumping at 350° C, interact with the tracer pulse at room temperature. In view of the dependency of the heat of chemisorption on surface coverage in this system (*11*), this is regarded as a surprisingly high figure.

The magnitude of the isotope effect on the amount adsorbed can be judged from a simple experiment. With Column III and at 0°C, some chromatograms were measured with hydrogen as carrier gas and deuterium as tracer. Then the deuterium cylinder was connected to the carrier gas line, and the column was flushed with D_2 for 1 hr at 90°C. Then runs were made at 0°C with D_2 as carrier gas and H_2 as tracer. Using average results for three carrier gas velocities, the following constants K_a were obtained:

(1) H_2 carrier, D_2 sample:
$K_a = 10.96 \pm 0.05$ (cm³/g)

(2) D_2 carrier, H_2 sample:
$K_a = 11.66 \pm 0.05$ (cm³/g)

It appears that the hydrogen atoms adhere a little more strongly on the nickel surface than the deuterium atoms. However, the isotope effect on the equilibrium is small.

Axial Diffusivity

According to Eqs. (16)–(18), plots of $(\mu_2 - t_0^2/12)/(2z/v)$ versus $1/v^2$ should give straight lines, if E_A and k_f are independent of the gas velocity. The slope and intercept of the lines are then equal to $E_A(1 + \delta_0)^2/\alpha$ and δ_1, respectively. Figures 3 to 5 show that the linear condition is fulfilled. With decreasing temperature the second moments increase considerably, but the scattering

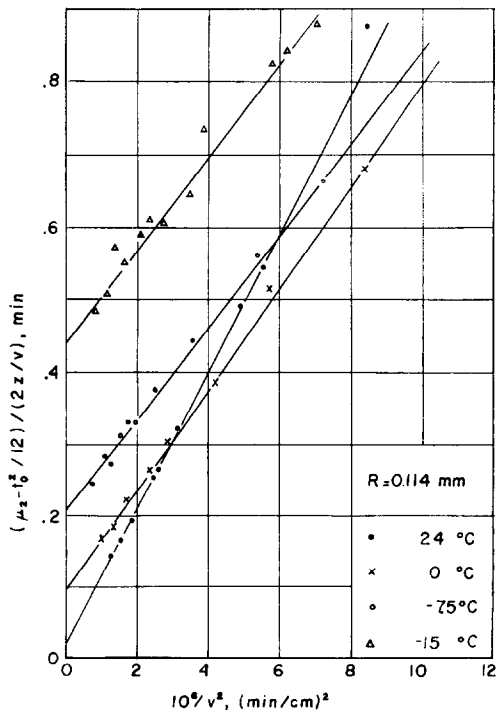

FIG. 3a. Second moment at high temperatures (Column I).

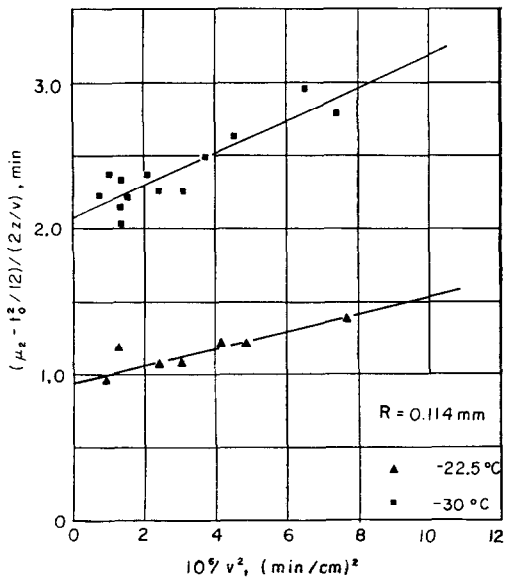

FIG. 3b. Second moment of low temperatures (Column I).

of the experimental points around the straight lines also increases. This is because the growing tails of the chromatographic peaks, which can be read with limited accuracy, contribute more and more to the

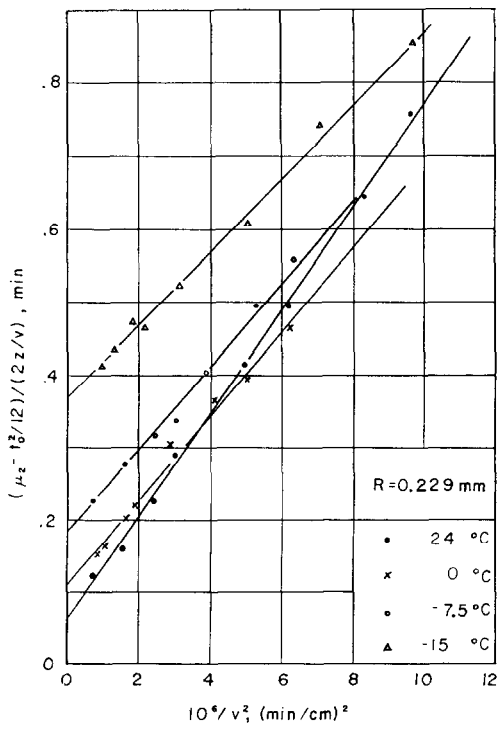

FIG. 4. Second moment (Column II).

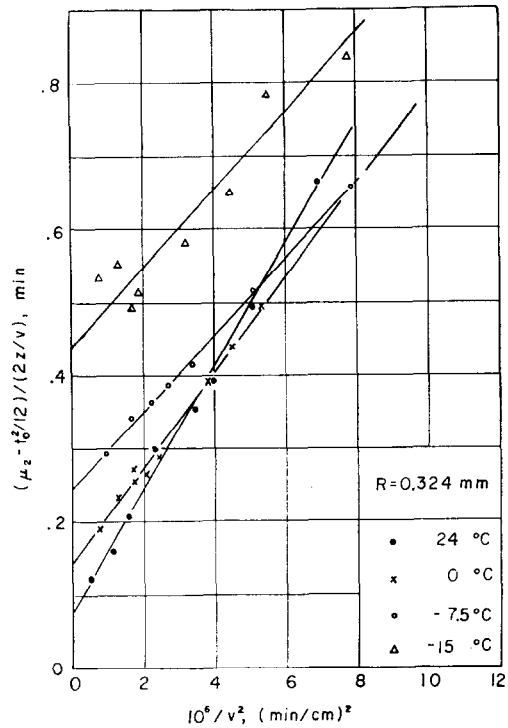

FIG. 5. Second moment (Column III).

second moments. This determined the lower limit of the temperature range in our experiments (−30°C).

The values of E_A calculated from the slopes may be related to the bulk diffusivity D_{AB} of the gas mixture according to $E_A = \alpha D_{AB}/q_{ext}$. Here q_{ext} is the external tortuosity factor. D_{AB} was calculated from the Chapman-Enskog theory for a mixture of HD and H_2, since this will be the prevailing mixture in the gas space of the column. The potential constants ϵ/k and σ_{AB} for HD were average values given by Hirschfelder (*13*) for H_2 and D_2. The values for E_A, D_{AB}, and q_{ext} are given in Table 5.

Since the values of q_{ext} are lower than expected (around 1.5), there might be some contribution to axial mixing from other mechanisms than molecular diffusion.

Intraparticle Diffusivity

The intercepts δ_1 from Figs. 3a, 4, and 5, divided by $(1-\alpha)\beta/\alpha$, are plotted against R^2 in Fig. 6. According to Eq. (18) straight lines should result with intercepts proportional to the adsorption rate resistance and slopes proportional to the diffusion

TABLE 5
AXIAL DIFFUSIVITIES

Temp. (°K):	297°	273°	265.5°	258°	250.5°	
D_{AB}(cm²/sec):	1.31	1.14	1.09	1.04	0.99	
			R = 0.114 mm			
E_A(cm²/sec)	0.489	0.368	0.334	0.336	0.318	$\bar{q}_{ext}$ = 1.13
q_{ext}	0.99	1.15	1.21	1.15	1.15	
			R = 0.229 mm			
E_A(cm²/sec)	0.468	0.395	0.389	0.340	—	$\bar{q}_{ext}$ = 1.13
q_{ext}	1.10	1.13	1.10	1.20	—	
			R = 0.324 mm			
E_A(cm²/sec)	0.518	0.413	0.332	0.357	—	$\bar{q}_{ext}$ = 1.11
q_{ext}	0.98	1.07	1.27	1.13	—	

resistance inside and around the particles [see Schneider (*1*) for detailed discussion]. At low gas velocities the latter resistance is that of normal bulk diffusion and the expression $k_f R$ in Eq. (18) can be replaced by D_{AB}. With D_{AB} = 1.14 cm²/sec (from Table 5) the intraparticle diffusivity D_c was calculated for 273°K from the slope of the appropriate line in Fig. 6. The result is

$$D_c = 1.25 \times 10^{-2} \text{ cm}^2/\text{sec}$$

Intraparticle diffusion resistance was a small fraction of that due to adsorption at nearly all temperatures. This is evident from the relatively large intercepts in Fig. 6. Hence the value for D_c is only an approximation. It is given for but one temperature, since the variation with temperature is less

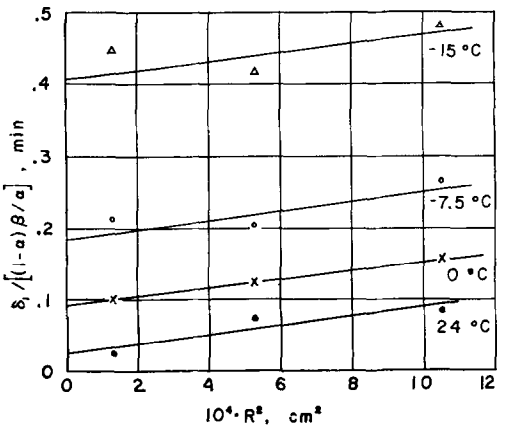

FIG. 6. Dependence of $\frac{\delta_1}{[(1-\alpha)/\alpha]\beta}$ upon particle size.

than the limit of error. The numerical value is typical of diffusivities expected for hydrogen in porous catalysts. For example, it may be compared with a value estimated, from the pore-geometry data given in Table 1. The equation

$$D_c = \frac{\beta_a^2}{(1/D_{AB}) + (1/D_{Ka})} + \frac{\beta_i^2(1+3\beta_a)}{(1-\beta_a)}\left[\frac{1}{(1/D_{AB}) + (1/D_{Ki})}\right] \quad (19)$$

given by Rao and Smith (*14*), may be used with D_{AB} = 1.14 cm²/sec. The Knudsen diffusivities for the micro- and macropores were calculated as

$$D_K = \tfrac{4}{3}\bar{r}\,(2R_gT/\pi M)^{\frac{1}{2}} \quad (20)$$

This approach gives $D_c = 2.5 \times 10^{-2}$ cm²/sec, which agrees with the experimentally established value to about the extent expected.

Rates of Adsorption and Desorption

Using Eq. (18), adsorption rate constants (k_a) were calculated from the intercepts in Fig. 6, down to a temperature of −15°C. For −22.5° and −30°C, chromatograms were obtained for only the smallest particle size. At these conditions diffusion resistance is negligible with respect to adsorption rate resistance and extrapolation to R = 0 is unnecessary. Hence k_a values for this particle size were calculated immediately from the intercepts in Fig. 3b. The results are given in Table 6. Multiplying k_a by the gas concentration (at 1 atm and the column

temperature) gives the total rates of adsorption and desorption of "hydrogen." Using the nickel surface area per gram of catalyst from Table 1 the rates may be expressed as molecules/(cm²)(sec). These rates are the major results of this work and are given in the last two rows of Table 6.

Figure 7 is an Arrhenius plot of the rates, and from the slope of the straight line an activation energy of 13.8 kcal/mole is calculated.

It is helpful to compare these results with the following theoretical equations:

$$r_a = C_g\left(\frac{n_s}{2}\right)\varphi_a(\theta)\frac{kT}{h}\frac{f^\ddagger}{F_g f_{s2}}\exp(-E_a/RT) \tag{21}$$

$$r_d = \left(\frac{n_s}{2}\right)\varphi_d(\theta)\frac{kT}{h}\frac{f^\ddagger}{f_{a2}}\exp(-E_d/RT) \tag{22}$$

These predictive equations follow from transition state theory for a diatomic molecule, adsorbed on the surface as immobile atoms. Considering the "total hydrogen" system, C_g is the total gas concentration at atmospheric pressure, and θ is the fractional surface coverage by both hydrogen and deuterium; $n_s/2$ is the maximum number of dual surface sites per cm² of the nickel surface. The function $\varphi_a(\theta)$ gives the probability that two neighboring sites are bare at a surface coverage θ; $\varphi_d(\theta)$ is the probability that pairs of atoms are adsorbed on adjacent sites; $f^\ddagger$ is the modified partition function of the activated complex, f_{s2} is the partition function for a dual surface site and f_{a2} is that for a pair of adsorbed atoms; F_g is the partition function for the gas per cm³.

If we consider Eq. (22), the experimental activation energy gives the combined temperature dependency of the single terms. The surface is nearly completely covered

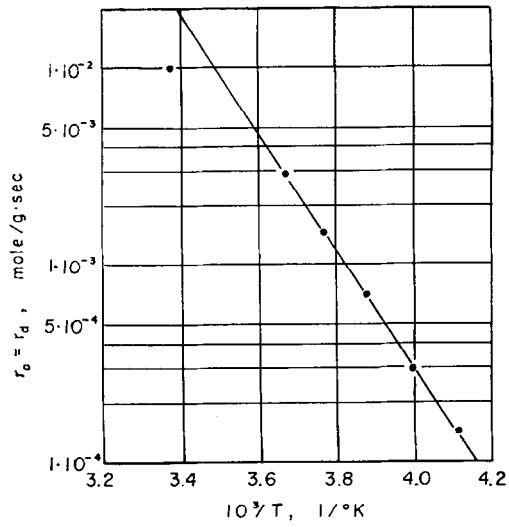

FIG. 7. Arrhenius plot for adsorption rates.

under our experimental conditions, and θ varies only slightly with temperature. Since the variation in θ will not cause a drastic change in $\varphi_d(\theta)$, and since this effect is partially compensated by the variation of kT/h with temperature, the experimental activation energy should be close to the true activation energy of desorption, E_d. Note that $r_a = r_d$ because equilibrium is established. For the isosteric heat of adsorption of hydrogen on nickel, using the chromatographic technique and a similar catalyst, Ozaki and co-workers (*4*) found $q = 13.5 \pm 1.5$ kcal/mole. Schuit and coworkers (*11*, *12*) give similar values for the heat of adsorption at higher surface coverage. Since $E_d = q + E_a$, this equality between E_d and the literature values for q suggests that the hydrogen adsorption on this nickel catalyst is nearly nonactivated. Then the rate of adsorption at equilibrium would be completely controlled by $\varphi_a(\theta)$.

These conclusions are partially confirmed

TABLE 6
ADSORPTION RATE RESULTS

Temp. (°K):	297°	273°	265.5°	258°	250.5°	243°
k_a(cm³/gsec)	244.2	64.9	32.1	14.54	6.10	2.85
$r_a = r_d$(mole/gsec)	1.0×10^{-2}	2.9×10^{-3}	1.47×10^{-3}	6.87×10^{-4}	2.98×10^{-4}	1.43×10^{-4}
$r_a = r_d$(molecules/cm² sec)	1.43×10^{16}	4.13×10^{15}	2.09×10^{15}	9.78×10^{14}	4.23×10^{14}	2.04×10^{14}

by evaluating Eqs. (21) and (22) numerically. We take $\varphi_d(\theta)$ in (22) approximately as 1. The adsorbed atoms and also the activated complexes are very likely to be immobile (*11, 12*). Hence the partition functions f^t, f_{a2}, and f_{s2} originate only from vibrations and therefore $f^t \approx f_{a2} \approx f_{s2} \approx 1$. The other numerical values are $n_s = 1.5 \times 10^{15}$ cm^{-2}, $kT/h = 5.7 \times 10^{12}$ sec^{-1}, and $\exp(-E_d/RT) = 0.885 \times 10^{-11}$ (at 273°K). From this the rate of desorption at 273°K is calculated to be $r_d = 3.8 \times 10^{16}$ molecules/cm^2 sec, which is in fairly good agreement with the experimental value of 4.13×10^{15} molecules/cm^2 sec from Table 6.

In Eq. (21) the partition function of the gas (HD, 273°K) is taken as $F_g = F_{tr} f_{rot} = 1.86 \times 10^{25}$ cm^{-3}. If we introduce the experimental value 4.13×10^{15} molecules/cm^2 sec on the left side of Eq. (21), the product $\varphi_a(\theta) \exp(-E_a/RT)$ is calculated to be 0.67×10^{-6}. Since $\varphi_a(\theta)$ must be a very small number for an almost completely covered surface, the activation energy of adsorption must be very small. This supports the conclusion drawn from the comparison of the experimental activation energy with the heat of adsorption.

So far the problem due to heterogeneity of the nickel surface for hydrogen chemisorption (*11, 12*) has been neglected. However, the conclusions already given are valid, if we follow the argument of Schuit and van Reijen (*11*). These authors assume that in this system the mechanisms on different parts of the surface are the same, and that all the surfaces are nearly saturated. Hence, the heterogeneity would result solely from a variation in activation energies (and heats of adsorption). Then the experimental activation energy has to be interpreted as an average value for the surface.

Conclusions

The results show that gas-solid chromatography can yield meaningful information on the rate of chemisorption, if an isotopic tracer can be used. Then the method gives the rates of adsorption and desorption in equilibrium between surface and gas. Knowledge of these may prove helpful in studying mechanisms of related catalytic reactions.

The same approach can be applied to other systems, provided a suitable detector for the analysis of the isotopic species in the chromatographic pulse is at hand.

Acknowledgment

Financial support from the Petroleum Research Fund, American Chemical Society, Grant #1633, is gratefully acknowledged.

References

1. Schneider, P., and Smith, J. M., *A.I.Ch.E. J.* **14**, 762 (1968).
2. Schneider, P., and Smith, J. M., *A.I.Ch.E. J.* to be published.
3. Ozaki, A., Nozaki, F., Maruya, K., and Ogasawara, S., *J. Catalysis* **7**, 234 (1967).
4. Ozaki, A., Shigehara, Y., and Ogasawara, S., *J. Catalysis* **8**, 22 (1967).
5. Laidler, K. J., "Chemical Kinetics." McGraw-Hill, New York, 1965.
6. Melander, L., "Isotope Effects on Reaction Rates." Ronald Press, New York, 1960.
7. Kubin, M., *Coll. Czech. Chem. Commun.* **30**, 1104 (1965).
8. Kubin, M., *Coll. Czech. Chem. Commun.* **30**, 2900 (1965).
9. Pierce, C., *J. Phys. Chem.* **57**, 149 (1953).
10. Hayward, D. O., and Trapnell, B. M. W., "Chemisorption." Butterworths, London, 1964.
11. Schuit, G. C. A., and van Reijen, L. L., *Advan. Catalysis* **10**, 135–137 (1958).
12. Schuit, G. C. A., de Boer, N. H., Dorgelo, G. J. H., and van Reijen, L. L., *in* "Chemisorption" (W. E. Garner ed.). Butterworths, London, 1967.
13. Hirschfelder, J. O., Curtiss, C. F., and Bird, R. B., "Molecular Theory of Gases and Liquids." Wiley, New York, 1954.
14. Rao, M. R., and Smith, J. M., *A.I.Ch.E. J.* **9**, 485 (1963).